PROCEEDINGS OF SPIE

SPIEDigitalLibrary.org/conference-proceedings-of-spie

Tuning of 2D rod-type photonic crystal cavity for optical modulation and impact sensing

Ogulcan E. Orsel, Mertcan Erdil, Cenk Yanik, Serdar Kocaman

Ogulcan E. Orsel, Mertcan Erdil, Cenk Yanik, Serdar Kocaman, "Tuning of 2D rod-type photonic crystal cavity for optical modulation and impact sensing

," Proc. SPIE 10931, MOEMS and Miniaturized Systems XVIII, 109310E (4 March 2019); doi: 10.1117/12.2509825

SPIE.

Event: SPIE OPTO, 2019, San Francisco, California, United States

Tuning of 2D Rod-Type Photonic Crystal Cavity for Optical Modulation and Impact Sensing

Ogulcan E. Orsel*[a],Mertcan Erdil [a],Cenk Yanik[b], Serdar Kocaman[a]
[a]Middle East Technical University, Üniversiteler Mahallesi, No: 1 06800 Çankaya Ankara/TURKEY; [b]Sabancı University, Orta Mahallesi, No:27, 34956 Tuzla/İstanbul/ TURKEY

ABSTRACT

We propose a novel way of mechanical perturbation of photonic crystal cavities for on-chip applications. We utilize the equivalence of the 2D photonic crystals with perfect electric conductor (PEC) boundary conditions to the infinite height 3D counterparts for rod type photonic crystals. Designed structures are sandwiched with PEC boundaries above and below and the perturbation of the cavity structures is demonstrated by changing the height of PEC boundary. Once a defect filled with air is introduced, the metallic boundary conditions is disturbed and the effective mode permittivity changes leading to a tuned optical properties of the structures. Devices utilizing this perturbation are designed for telecom wavelengths and PEC boundaries are replaced by gold plates during implementation. For 10 nm gold plate displacement, two different cavity structures showed a 21.5 nm and 26 nm shift in the resonant wavelength. Optical modulation with a 1.3 MHz maximum modulation frequency with a maximum power consumption of 36.81 nW and impact sensing with 20 μs response time (much faster compared to the commercially available ones) are shown to be possible.

Keywords: Photonic crystal, metallic perturbation, opto-mechanical interaction

1. INTRODUCTION

Recent discoveries on opto-mechanical interactions opened a new era for photonic sensors and systems. With the advances in nanofabrication, experimental realization of these interactions have been demonstrated in many studies.[1-12]. Some concrete examples can be given as single photon frequency shifters[13], utilizing vibration in order to introduce nonlinear effects and quantum cooling effects which can be used to incorporate self-cooling chips [14, 15]. Moreover, detection of radio waves by displacement of Al-coated SiN membrane [16] is demonstrated as auspicious optical detectors and concurrently, novel optical gyroscopes are designed [17, 18] .Hence, mechanics and photonics are uniting disciplines for the production of novel structures that are necessity for challenging situations. Many authors proposed ways to tune characteristics of the structure of a thermo-optic, electro-optic and opto-mechanic systems. These changes are seen to be mainly on the refractive index of the medium. For instance, thermo-optic systems incorporate heat for that change. Utilization of thermo-optic effects is usually made possible by placing metallic heaters in the proximity of structure of interest [19]. However, interaction of guided mode with these metallic heaters results in low transmittance, so additional layer is being inserted between waveguide and metal layers [20]. This additional layer enables mode propagation by decreasing the mode overlap with the metallic heaters. Even though this additional layer, thermo-optic effects have higher tuning range. However, they suffer from high power consumption and limited operating speeds due to thermal capacitance of the structure. Electro-optic systems are faster when compared to the thermo-optic systems. However, high voltages are required for small tuning ranges [21, 22]. One class of electro-optic effects use p-n or p-i-n junctions to inject carries [23-29]. Even though the power consumption is decreased and the carrier injection produces relatively high refractive index changes, the thermal characteristics of the devices are not considered. Heat generation due to carrier injection, changes the characteristic of the system substantially compared to the carrier injection. In order to prevent the excessive heating, another class of electro-optic effects use MOS structure [30-32] and eliminates the heat generation of the system by MOS capacitor. Nowadays, plasmon assisted electro-optic effects are used for modulator designs [33-37] and layered graphene based structures are proposed and designed as emerging technologies [38-44]. Additionally, strain effect on silicon's refractive index is shown to be effective enough to practice it as a sensor [45, 46].

MOEMS and Miniaturized Systems XVIII, edited by Wibool Piyawattanametha, Yong-Hwa Park, Hans Zappe,
Proc. of SPIE Vol. 10931, 109310E · © 2019 SPIE · CCC code: 0277-786X/19/$18 · doi: 10.1117/12.2509825

On the opto-mechanical side, mechanical deformation or actuation of the subparts of photonic systems are used in order to incorporate evanescent coupling. Most frequently used ones are cavity structures or parallel waveguides. The perturbation of the evanescent fields can produce large change in the characteristics of the system with small voltages. By changing the field, the effective refractive index of the structure changes and that results in resonant shift of the system or phase shift of the incoming light. Some types use parallel high dielectric waveguides and plate structures [47-56] and incorporates NEMS actuators to change the coupling between the waveguide, whereas other types use ring resonators and deforms the structure out of plane and in plane [57-62] by capacitive actuators. In this work, mechanical perturbation of photonic crystal cavities for on-chip applications is demonstrated. The effective mode permittivity is shown to be changed by first disturbing infinite rod height for PhC slab cavity which is bounded by PECs. Later, the same boundaries are replaced by gold plates for practical applications and same effect is observed. This way a novel opto-mechanical coupling of rod type PhCs is introduced and explained.

2. CAVITY STRUCTURE

In order to show the effect of permittivity disturbance that leads opto-mechanical coupling, a two dimensional PhC cavity side coupled to a line defect waveguide is designed. The structure is constructed in hexagonal lattice formation, where the lattice constant a=610 nm and hole radius r=0.2a. The design parameters are selected in order to maximize the Q-factor of resonant mode inside the cavity. The transmission of side coupled cavity around resonance is numerically analyzed via 2D FEM simulations and it is given in the Fig.1 (a).

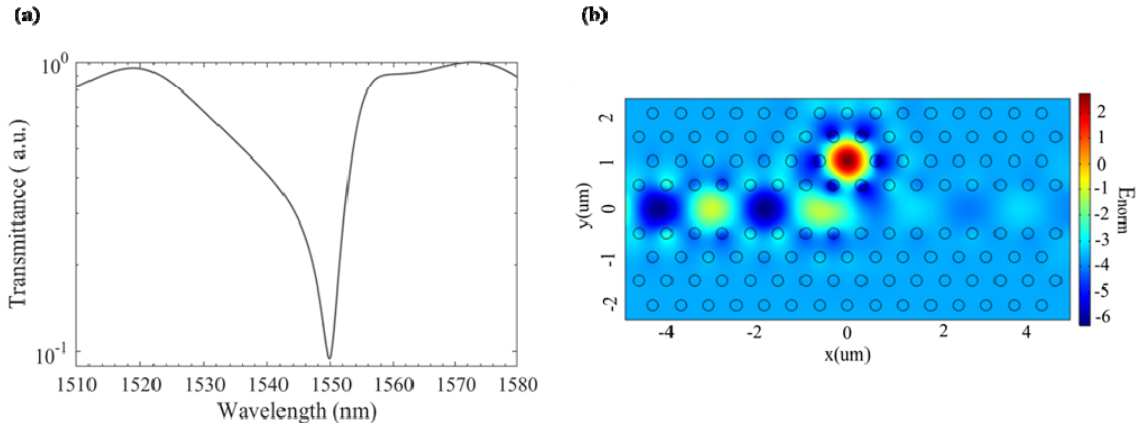

Figure 1. (a) Transmission of the side coupled cavity vs. wavelength. (b) Side coupled cavity at its resonant wavelength of 1550 nm.

Referring to the Fig. 1(a), structure has a resonance around 1550 nm wavelength for TM excitation. Resonant mode profile inside the cavity is presented in Fig. 1(b). The cavity structure inhibits discrete translational symmetry in x and y directions and continuous translational symmetry in z direction as the structure extends to infinity in z direction for 2D analysis, meaning that the effective rod height for TM modes are infinity. It is still possible to implement 2D photonic crystal structure by implementing PEC boundary conditions to a 3D slab. In this case, k_z vector is being forced to zero and hence TM modes similarly sees infinite height of rods. But, TE modes are changed, and they are shifted to higher frequencies, due to the boundary condition, forced by the PEC which ensures that $E_{//}$ to the conductor surface is equal to zero. Now, a question arises whether it is possible to change the permittivity of the PhC such that it leads to a controlled tuning of the system. The main idea of designing photonic crystals is to have a permittivity that is function of space. So, this idea can be applied to the slab photonic crystals such that the permittivity map of the device is being changed in the out of plane direction while ensuring the semi-infinite rod height which acts like a 3D photonic crystal. This new form of crystal has a periodicity in the z direction such that by the insertion of the air gap decreases the effective mode index. As it can be observed in Fig. 1(b), the resonant mode of the cavity is localized in air region. From small perturbation of the dielectric function,

$$\Delta\omega = -\frac{\omega \int d^3\boldsymbol{r}\Delta\varepsilon(\boldsymbol{r})|\boldsymbol{E}(\boldsymbol{r})|^2}{2 \int d^3\boldsymbol{r}\varepsilon(\boldsymbol{r})|\boldsymbol{E}(\boldsymbol{r})|^2} + O(\Delta\varepsilon^2) \quad (1)$$

From (1), as the dielectric function is decreased, mode frequencies are shifted to the higher frequencies. The perturbation in the out of plane direction is possible if the TM waves still see infinite height of rods. This can be done by the mechanical disturbance of the PEC boundary.

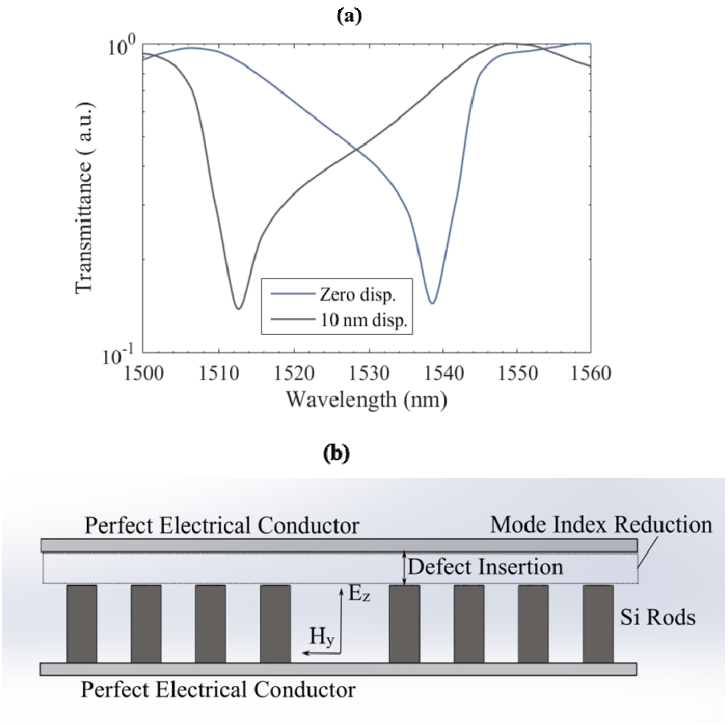

Figure 2. (a) Resonant shift of the side coupled cavity via permittivity perturbation. (b) 3-D slab PhC with PEC boundary conditions for the top and bottom plate.

Mechanical perturbation of PEC boundary is being accomplished by creating an air defect between the top of the rods and the metal surface. In a different perspective, air rods are created on top of the silicon rods such that this semi-infinite height silicon photonic crystal acts as if the PhC permittivity is changing in the z direction while satisfying the infinite rod height. By that way, properties of the PhC is disturbed in a controlled manner. In Fig. 2, the resonant shift of the system is apparent and it is interesting to note that even the rod height is increased while maintaining the PEC boundaries, the system properties are not disturbed. On the other hand, braking the translational symmetry in z direction by the insertion of air defect makes rod height as an important parameter. Since, in this case rods are not infinite although the PhC carries same modes as in the 2D case, and the system obeys equation (1). Moreover, it is observed that, the resonant frequencies of the side coupled cavity is shifted by 26 nm. Remembering that the cavity modes are supported by mostly air, the results of the mode shapes for the cavity in transverse plane are pretty interesting and they are given in the Fig.3.

By comparing Fig. 3(a)-(b), one can see the effect of perturbation on the mode profile of the cavity. When the air defect is introduced, light localizes in the defect, making the structure strongly sensitive to the geometrical perturbations. Mode shapes in Fig. 3 (a)-(b) are in agreement with the equation (1) i.e. the effective permittivity of the mode is decreased, leading to a blue shifted resonant frequency. For practical applications, Gold plates will be used instead of the ideal PEC boundary conditions. In order to explain the effect of the gold on the system, it is vital to analyze the gold structure itself. Thus, the transmittance and reflectance of 50 nm flat gold layer between two air regions is investigated. Simulation is done in 2-D and the structure is excited by TM waves. The results of absorption and reflection of Gold layers are given in the Fig. 4(a)-(b), respectively.

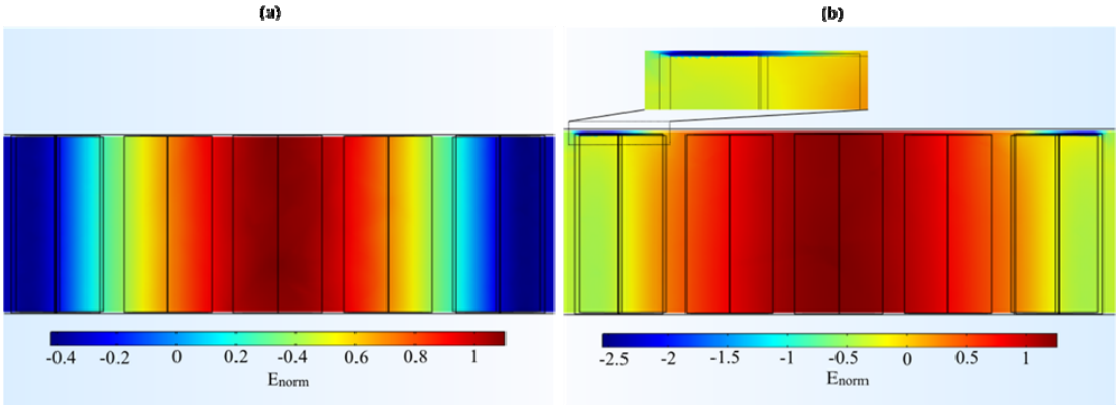

Figure 3. (a) Mode shape of the undisturbed cavity (b) Mode shape of the disturbed cavity (Note that the scales of the normalized E_z components are done on the same basis)

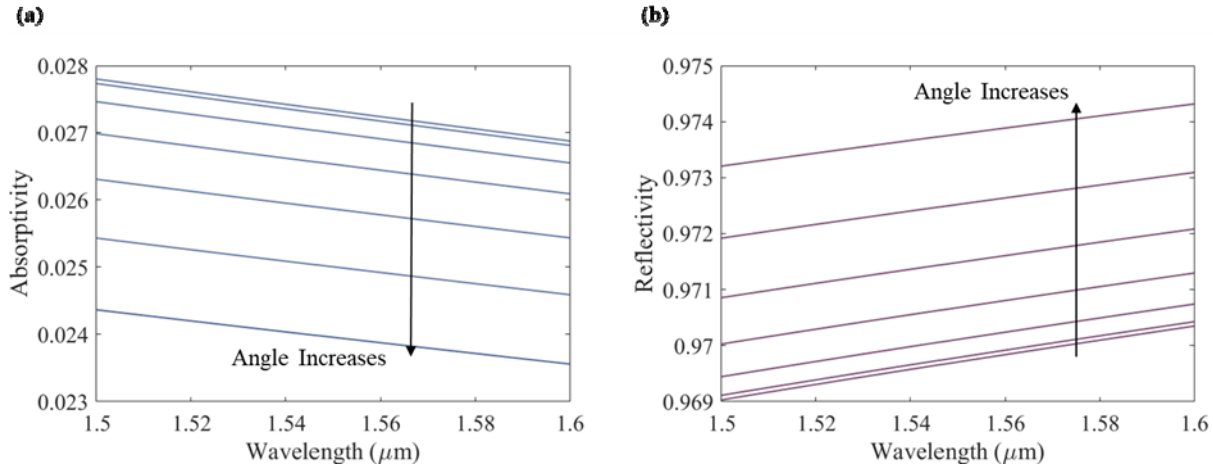

Figure 4. (a) Absorptivity of the flat gold surface for different angles and frequencies (b) Reflectivity of the gold flat surface for different angles and frequencies (Angle is varied from 0˚ to 30˚ with 5˚ steps)

Referring to the Fig. 4, the reflection from the gold surface is high and it is decreasing by increasing the input frequency. Similarly, the penetration depth into the gold surface is also increasing with the increased absorptivity and that results in a dissipative behavior. That behavior is apparent due to the frequency dependent conductivity of the gold. The permittivity of the gold changes on account of the conductivity change and that is often explained with the Drude-Sommerfeld model [65]**.** The complex permittivity of the gold is given as,

$$\varepsilon(\omega) = \varepsilon_0 - \frac{\omega_p^2}{\omega^2 + i\Upsilon_{bulk}\omega} \quad (2)$$

In (2), ω_p is the bulk plasma frequency, Υ_{bulk} is proportional to the reciprocal of the mean free time between electron collision times [66] and ε_0 represents the effect of interband transitions to the polarizability [67-69]. From equation (2), as the real part of ε becomes zero, metal reaches its bulk plasma frequency and it reaches its surface plasma frequency at $1/\sqrt{2}$ of the bulk plasma frequency. In our design, gold is far below its plasma frequency and resonances occur as in the 2-D case. As the real part of (2) sustains to be negative, gold is still a good reflector, however it is not a PEC. At $\omega = 0$, the permittivity is $-\infty$ and one can presume that the absolute value of the permittivity is decreasing leading to an increased modal frequencies for PhC. Hence, it is going to affect the resonant frequencies due to the non-ideal conductor boundary. Moreover, since there exists dissipation thorough the gold plates, the transmission reduces. To

show that, same structures as in the Fig. 2 is investigated by replacing PEC boundaries with 50 nm gold plates and the results are given in the Fig. 5(a).

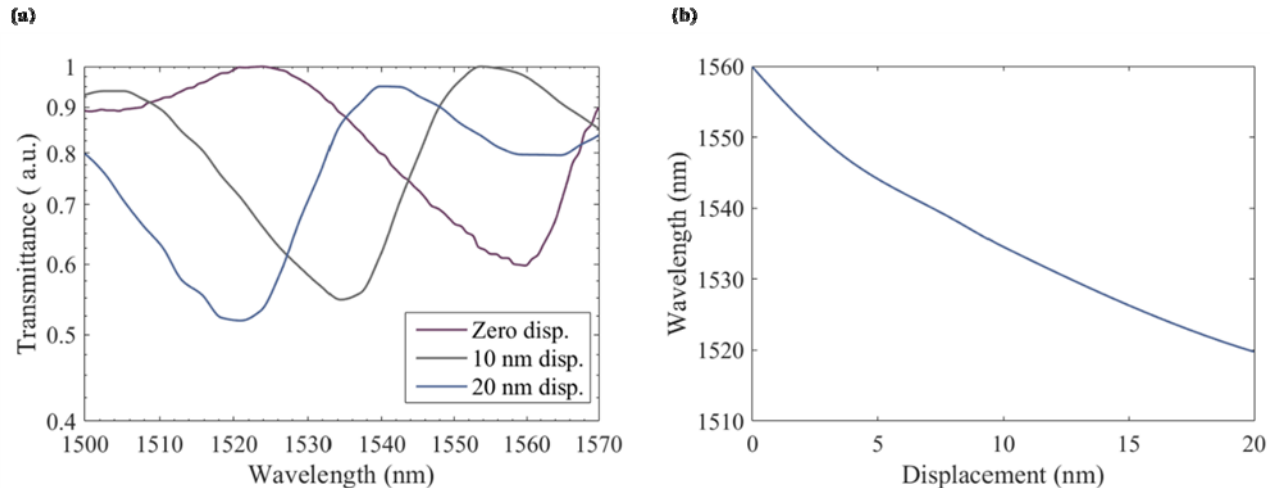

Figure 5. (a) Resonant shift of the side coupled cavity for gold plate boundary conditions. (b) Resonant shift of the cavity with different air defect heights.

From Fig. 5a, the transmission of the side coupled slightly changed and the change in the resonant wavelength is also shown. Moreover, Fig. 5b shows the resonant shift of the side coupled cavity with respect to various displacements and this behavior can be perceived as piecewise linear. The system effectively shows the same behavior that is predicted by equation (1) which is linear in terms of $\Delta\varepsilon$ and this indeed shows that the rods of the PhC see near infinite rods such that the controlled tuning of the PhC properties are possible. Additionally, the lattice constant of the rods for PEC case and gold plate cases are different from each other. For PEC boundary, lattice constant is 610 nm, on the other hand it is 577nm for gold boundaries. That is apparent owing to the perturbation created by the gold plates which have finite permittivity on the system.

3. OPTOMECHANICS AND APPLICATIONS

Design of the optomechanical structure is completed by taking practical concerns into consideration and it is shown in Fig. 6. Two layers of gold is being used and bottom gold layer is designed to pull the top plate by electrostatic actuation. In order to eliminate the heating of the structure, SOI wafer is used and the system dissipates power if an AC voltage is applied between top and bottom gold layers. That dissipation is due to the change of the energy of the capacitance between top and bottom layers. There are no electrical connection for the gold layer that is at the bottom of the PhC. Depending on the heights of the stepped structure, system can be either used as modulator or inertial sensor. Since, the system is going to be used in atmospheric conditions and air between the gold plate and PhC needs to be analyzed. The vibration analysis of the gold plate with the fluidic damping is done and it is used in the following analyses.

Considering Fig. 5a and 6, the top plate can be actuated by 10 nm and that will shift the characteristic of the structure considerably. Using that idea, 100 nm displacement between PhC and gold plate is given. Because of deposition of gold, there will be 50 nm gold layer on the top of the PhC cylinders. That will result in 50 nm actuating length of the top plate. Additionally, 200 nm distance is set for the bottom gold layer and top gold layer. For the least possible power consumption, firstly the top plate is being pulled by 40 nm via DC voltage applied between bottom gold layer and top gold layer. Then, AC voltage is applied between bottom gold layer and top gold layer. The system is a nonlinear one since there exists gap nonlinearity between top plate and PhC. Gap non-linearity is being put intentionally to prevent excessive vibration of the plate at resonant frequency. Non-linear system is modelled as SDOF and analyzed in terms of its time response for modulation speed. The modulation frequency can go up to 1.3 MHz and for that purpose, response of the system for 1μs pulse is given. Initially 8.45 Volt is being applied between top and bottom gold

layers and 0.5 Volts is being applied as modulation voltage. The system dissipates power whenever 0.5 Volts AC voltage is applied on account of capacitive action. So the power consumption of the system becomes 28.34 nW under 50 % duty cycle and 1 MHz modulation frequency. The proposed modulator design has low modulation frequency but it has relatively small power consumption [70-72].

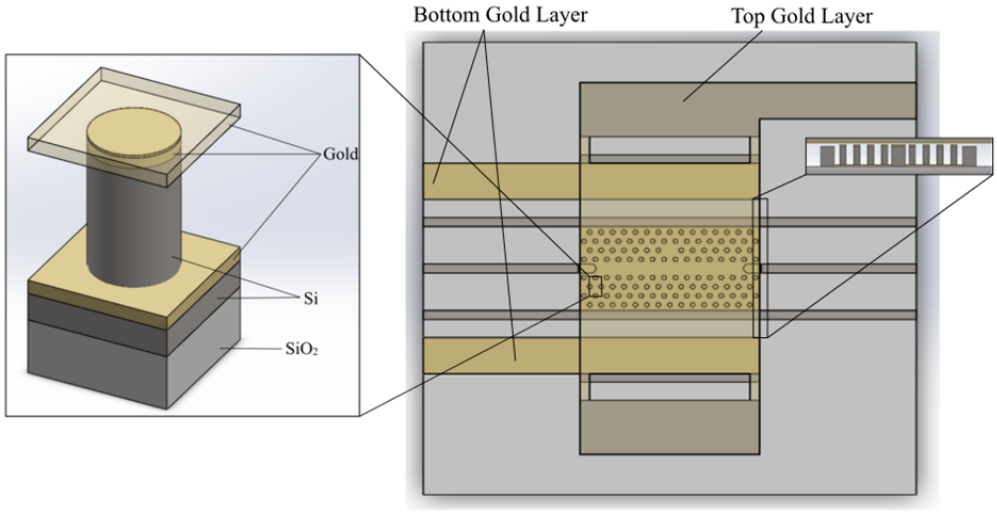

Figure 6. Designed structure

Proposed structure can also be used as inertial sensor and especially impact sensor. For that purpose, gap between PhC and top plate should be changed in order to make use of the pull-in property of capacitive actuation. Moreover, similar non-linearity that is gap non-linearity is used in order to prevent excessive current due to pull-in. By that way, sensitivity of the mechanical structure is increased by operating it near the pull-in displacement and it can be modified for different kind of impact situations by adjusting DC voltage between top and bottom gold layer. For automobile crash accidents, the peak acceleration is around 25g. Thus, the dimensions are changed (increasing the length of the beams and deposition more gold for top plate) for detection of the low g accelerations. The response time of the system is found to be around 20 μs and this is a much higher response time that is presented [73] for low g applications. Since, the detection of the crash will be based on light, side coupled cavity will reach steady state much faster than the mechanical structure.

REFERENCES

[1] Thompson, J. et al. Strong dispersive coupling of a high-finesse cavity to a micromechanical membrane. *Nature* 452, 900-900 (2008).

[2] Eichenfield, M., Camacho, R. , Chan, J. , Vahala, K. & Painter, O. A picogram- and nanometre-scale photonic-crystal optomechanical cavity. *Nature* 459, 550-555 (2009).

[3] Eichenfield, M., Chan, J., Camacho, R., Vahala, K. & Painter, O. Optomechanical crystals. *Nature* 462, 78-82 (2009).

[4] Verhagen, E., Deléglise, S., Weis, S., Schliesser, A. & Kippenberg, T. Quantum-coherent coupling of a mechanical oscillator to an optical cavity mode. *Nature* 482, 63-67 (2012).

[5] Safavi-Naeini, A. et al. Squeezed light from a silicon micromechanical resonator. *Nature* 500, 185-189 (2013).

[6] Wilson, D. et al. Measurement-based control of a mechanical oscillator at its thermal decoherence rate. *Nature* 524, 325-329 (2015).

[7] Favero, I. & Karrai, K. Optomechanics of deformable optical cavities. *Nature Photonics* 3, 201-205 (2009).
[8] Marin-Palomo, P. et al. Microresonator-based solitons for massively parallel coherent optical communications. *Nature* 546, 274-279 (2017).
[9] Li, M., Pernice, W. & Tang, H. Tunable bipolar optical interactions between guided lightwaves. *Nature Photonics* 3, 464-468 (2009).
[10] Lin, Q. et al. Coherent mixing of mechanical excitations in nano-optomechanical structures. *Nature Photonics* 4, 236-242 (2010).
[11] Balram, K., Davanço, M., Song, J. & Srinivasan, K. Coherent coupling between radiofrequency, optical and acoustic waves in piezo-optomechanical circuits. *Nature Photonics* 10, 346-352 (2016).
[12] Gröblacher, S., Hammerer, K., Vanner, M. & Aspelmeyer, M. Observation of strong coupling between a micromechanical resonator and an optical cavity field. *Nature* 460, 724-727 (2009).
[13] Fan, L. et al. Integrated optomechanical single-photon frequency shifter. *Nature Photonics* 10, 766-770 (2016).
[14] Clark, J., Lecocq, F., Simmonds, R., Aumentado, J. & Teufel, J. Sideband cooling beyond the quantum backaction limit with squeezed light. *Nature* 541, 191-195 (2017).
[15] Arcizet, O., Cohadon, P., Briant, T., Pinard, M. & Heidmann, A. Radiation-pressure cooling and optomechanical instability of a micromirror. *Nature* 444, 71-74 (2006).
[16] Bagci, T. et al. Optical detection of radio waves through a nanomechanical transducer. *Nature* 507, 81-85 (2014).
[17] Srivastava, S., Rao D. S., S. & Nandakumar, H. Novel optical gyroscope: proof of principle demonstration and future scope. *Scientific Reports* 6, (2016).
[18] Wu, B., Yu, Y., Xiong, J. & Zhang, X. Silicon Integrated Interferometric Optical Gyroscope. *Scientific Reports* 8, (2018).
[19] Pruessner, M., Stievater, T., Ferraro, M. & Rabinovich, W. Thermo-optic tuning and switching in SOI waveguide Fabry-Perot microcavities. *Optics Express* 15, 7557 (2007).
[20] Yamane, T., Nagai, N., Katayama, S.-I. & Todoki, M. Measurement of thermal conductivity of silicon dioxide thin flms using a 3ω method. *Journal of Applied Physics* **91**, 9772 (2002).
[21] Scrymgeour, D., Malkova, N., Kim, S. & Gopalan, V. Electro-optic control of the superprism effect in photonic crystals. *Applied Physics Letters* 82, 3176-3178 (2003).
[22] Atabaki, A. et al. Integrating photonics with silicon nanoelectronics for the next generation of systems on a chip. *Nature* 556, 349-354 (2018).
[23] Jiang, Y., Jiang, W., Gu, L., Chen, X. & Chen, R. 80-micron interaction length silicon photonic crystal waveguide modulator. *Applied Physics Letters* 87, 221105 (2005).
[24] Xu, Q., Schmidt, B., Pradhan, S. & Lipson, M. Micrometre-scale silicon electro-optic modulator. *Nature* 435, 325-327 (2005).
[25] Vlasov, Y., O'Boyle, M., Hamann, H. & McNab, S. Active control of slow light on a chip with photonic crystal waveguides. *Nature* 438, 65-69 (2005).
[26] Liu, J. et al. Waveguide-integrated, ultralow-energy GeSi electro-absorption modulators. *Nature Photonics* 2, 433-437 (2008).
[27] Wolf, S. et al. Silicon-Organic Hybrid (SOH) Mach-Zehnder Modulators for 100 Gbit/s on-off Keying. *Scientific Reports* 8, (2018).
[28] Govdeli, A., Sarihan, M., Karaca, U. & Kocaman, S. Integrated Optical Modulator Based on Transition between Photonic Bands. *Scientific Reports* 8, (2018).
[29] Long, Y., Zhou, L. & Wang, J. Photonic-assisted microwave signal multiplication and modulation using a silicon Mach–Zehnder modulator. *Scientific Reports* 6, (2016).
[30] Liu, A. et al. A high-speed silicon optical modulator based on a metal–oxide–semiconductor capacitor. *Nature* 427, 615-618 (2004).

[31] Hiraki, T. et al. Heterogeneously integrated III–V/Si MOS capacitor Mach–Zehnder modulator. *Nature Photonics* 11, 482-485 (2017).
[32] Han, J. et al. Efficient low-loss InGaAsP/Si hybrid MOS optical modulator. *Nature Photonics* 11, 486-490 (2017).
[33] Melikyan, A. et al. High-speed plasmonic phase modulators. *Nature Photonics* 8, 229-233 (2014).
[34] Dennis, B. et al. Compact nanomechanical plasmonic phase modulators. *Nature Photonics* 9, 267-273 (2015).
[35] Haffner, C. et al. All-plasmonic Mach–Zehnder modulator enabling optical high-speed communication at the microscale. *Nature Photonics* 9, 525-528 (2015).
[36] Woessner, A. et al. Electrical 2π phase control of infrared light in a 350-nm footprint using graphene plasmons. *Nature Photonics* 11, 421-424 (2017).
[37] Haffner, C. et al. Low-loss plasmon-assisted electro-optic modulator. *Nature* 556, 483-486 (2018).
[38] Liu, M. et al. A graphene-based broadband optical modulator. *Nature* 474, 64-67 (2011).
[39] Kim, K., Choi, J., Kim, T., Cho, S. & Chung, H. A role for graphene in silicon-based semiconductor devices. *Nature* 479, 338-344 (2011).
[40] Novoselov, K. et al. A roadmap for graphene. *Nature* 490, 192-200 (2012).
[41] Phare, C., Daniel Lee, Y., Cardenas, J. & Lipson, M. Graphene electro-optic modulator with 30 GHz bandwidth. *Nature Photonics* 9, 511-514 (2015).
[42] Sun, Z., Martinez, A. & Wang, F. Optical modulators with 2D layered materials. *Nature Photonics* 10, 227-238 (2016).
[43] Sorianello, V. et al. Graphene–silicon phase modulators with gigahertz bandwidth. *Nature Photonics* 12, 40-44 (2017).
[44] Yao, B. et al. Gate-tunable frequency combs in graphene–nitride microresonators. *Nature* 558, 410-414 (2018).
[45] Jacobsen, R. et al. Strained silicon as a new electro-optic material. *Nature* 441, 199-202 (2006).
[46] Kim, Y., Takenaka, M., Osada, T., Hata, M. & Takagi, S. Strain-induced enhancement of plasma dispersion effect and free-carrier absorption in SiGe optical modulators. *Scientific Reports* 4, (2014).
[47] Bulgan, E., Kanamori, Y. & Hane, K. Submicron silicon waveguide optical switch driven by microelectromechanical actuator. *Applied Physics Letters* 92, 101110 (2008).
[48] Poot, M. & Tang, H. Broadband nanoelectromechanical phase shifting of light on a chip. *Applied Physics Letters* 104, 061101 (2014).
[49] Van Acoleyen, K. et al. Ultracompact Phase Modulator Based on a Cascade of NEMS-Operated Slot Waveguides Fabricated in Silicon-on-Insulator. *IEEE Photonics Journal* 4, 779-788 (2012).
[50] Abe, S., Chu, M., Sasaki, T. & Hane, K. Time Response of a Microelectromechanical Silicon Photonic Waveguide Coupler Switch. *IEEE Photonics Technology Letters* 26, 1553-1556 (2014).
[51] Akihama, Y. & Hane, K. An analytical coupling coefficient for MEMS tunable silicon nanowire waveguide coupler devices. *Microsystem Technologies* 19, 583-589 (2012).
[52] Akihama, Y. & Hane, K. Single and multiple optical switches that use freestanding silicon nanowire waveguide couplers. *Light: Science & Applications* 1, e16-e16 (2012).
[53] Chollet, F. Devices Based on Co-Integrated MEMS Actuators and Optical Waveguide: A Review. *Micromachines* 7, 18 (2016).
[54] Abdulla, S. et al. Tuning a racetrack ring resonator by an integrated dielectric MEMS cantilever. *Optics Express* 19, 15864 (2011).
[55] Akihama, Y., Kanamori, Y. & Hane, K. Ultra-small silicon waveguide coupler switch using gap-variable mechanism. *Optics Express* 19, 23658 (2011).
[56] Erdil, M., Ozer, Y. & Kocaman S., High-Q Slot Mode Photonic Crystal Nanobeam Cavity with Optomechanically Enhanced Sensitivity, IEEE Journal of Selected Topics in Quantum Electronics (2019)
[57] Lee, M. & Wu, M. MEMS-actuated microdisk resonators with variable power coupling ratios. *IEEE Photonics Technology Letters* 17, 1034-1036 (2005).

[58] Yao, J., Leuenberger, D., Lee, M. & Wu, M. Silicon Microtoroidal Resonators With Integrated MEMS Tunable Coupler. *IEEE Journal of Selected Topics in Quantum Electronics* 13, 202-208 (2007).
[59] Kanamori, Y., Sato, Y. & Hane, K. Fabrication of Silicon Microdisk Resonators with Movable Waveguides for Control of Power Coupling Ratio. *Japanese Journal of Applied Physics* 52, 06GL19 (2013).
[60] Lee, M. & Wu, M. Tunable coupling regimes of silicon microdisk resonators using MEMS actuators. *Optics Express* 14, 4703 (2006).
[61] Sridaran, S. & Bhave, S. Electrostatic actuation of silicon optomechanical resonators. *Optics Express* 19, 9020 (2011).
[62] Hermouet, M. et al. 1 Million-Q Optomechanical Microdisk Resonators with Very Large Scale Integration. *Proceedings* 1, 347 (2017).
[63] Guo, X., Zou, C., Ren, X., Sun, F. & Guo, G. Broadband opto-mechanical phase shifter for photonic integrated circuits. *Applied Physics Letters* 101, 071114 (2012).
[64] Ozer, Y. & Kocaman, S. Stability Formulation for Integrated Opto-mechanic Phase Shifters. *Scientific Reports* 8, (2018).
[65] Derkachova, A., Kolwas, K. & Demchenko, I. Dielectric Function for Gold in Plasmonics Applications: Size Dependence of Plasmon Resonance Frequencies and Damping Rates for Nanospheres. *Plasmonics* 11, 941-951 (2015).
[66] Sonnichen C, Franzl T, Wilk T, von Plessen G, Fe J (2002) ¨ Plasmon resonances in large noble-metal clusters. New J Phys
4:93.1–93.8
[67] Oubre C, Nordlander P (2004) Optical properties of metallodielectric nanostructures calculated using the finite difference time domain method. J Phys Chem B 108:17740–17747
[68] Sonnichsen C (2001) Plasmons in metal nanostructures. Ph.D. ¨ thesis, Ludwig-Maximilians-Universitat Munchen
[69] Grady N, Halas N, Nordlander P (2004) Influence of dielectric function properties on the optical response of plasmon resonant metallic nanoparticles. Chem Phys Lett 399:167–171
[70] Xin, M., Danner, A., Png, C. & Lim, S. Resonator-Based Silicon Electro-Optic Modulator with Low Power Consumption. *Japanese Journal of Applied Physics* 48, 04C104 (2009).
[71] Miller, D. Energy consumption in optical modulators for interconnects. *Optics Express* 20, A293 (2012).
[72] Timurdogan, E. et al. An ultralow power athermal silicon modulator. *Nature Communications* 5, (2014).
[73] Sinha, S., Gopal, R. & Mukhiya, R. Design and Simulation of MEMS Differential Capacitive Accelerometer. (2014). doi:10.13140/2.1.1074.8809